# Structural diversity and electronic properties of $Cu_2SnX_3$ ($X$ = S, Se): A first-principles investigation

Ying-Teng Zhai,[1] Shiyou Chen,[2] Ji-Hui Yang,[1] Hong-Jun Xiang,[1] Xin-Gao Gong,[1] Aron Walsh,[3] Joongoo Kang,[4] and Su-Huai Wei[4]

[1]*Key Laboratory for Computational Physical Sciences (MOE) and Surface Physics, Fudan University, Shanghai 200433, China*
[2]*Key Laboratory of Polar Materials and Devices (MOE), East China Normal University, Shanghai 200241, China*
[3]*Centre for Sustainable Chemical Technologies and Department of Chemistry, University of Bath, Claverton Down, Bath BA2 7AY, United Kingdom*
[4]*National Renewable Energy Laboratory, Golden, Colorado 80401, USA*

(Received 23 May 2011; revised manuscript received 11 July 2011; published 15 August 2011)

The ternary semiconductors $Cu_2SnX_3$ ($X$ = S, Se) are found frequently as secondary phases in synthesized $Cu_2ZnSnS_4$ and $Cu_2ZnSnSe_4$ samples, but previous reports on their crystal structures and electronic band gaps are conflicting. Here we report their structural and electronic properties as calculated using a first-principles approach. We find that (i) the diverse range of crystal structures such as the monoclinic, cubic, and tetragonal phases can all be derived from the zinc-blende structure with tetrahedral coordination. (ii) The energy stability of different structures is determined primarily by the local cation coordination around anions, which can be explained by a generalized valence octet rule. Structures with only $Cu_3Sn$ and $Cu_2Sn_2$ clusters around the anions have low and nearly degenerate energies, which makes Cu and Sn partially disordered in the cation sublattice. (iii) The direct band gaps of the low-energy compounds $Cu_2SnS_3$ and $Cu_2SnSe_3$ should be in the range of 0.8–0.9 and 0.4 eV, respectively, and are weakly dependent on the long-range structural order. A direct analogy is drawn with the ordered vacancy compounds found in the $Cu(In,Ga)Se_2$ solar-cell absorbers.

DOI: 10.1103/PhysRevB.84.075213 PACS number(s): 61.50.Ah, 71.20.Nr, 71.22.+i, 71.70.Fk

## I. INTRODUCTION

As candidates for low-cost thin-film solar-cell absorbers, quaternary semiconductors $Cu_2ZnSnS_4$ (CZTS) and $Cu_2ZnSnSe_4$ (CZTSe) have been studied intensively in the past five years.[1–6] Due to the increased number of elements in the materials, their synthesis is relatively more difficult than for binary and ternary semiconductors[7,8] because more secondary phases such as ZnS, $Cu_2SnS_3$ (CTS), ZnSe, and $Cu_2SnSe_3$ (CTSe) may coexist in the samples.[9,10] The coexistence of these secondary phase compounds will inevitably influence the electrical and optical properties of CZTS and CZTSe samples, which have been observed experimentally and taken as the reason for the scattering of the measured properties.[11]

Despite a long history of the experimental study of CTS and CTSe ternary compounds, their fundamental properties such as the crystal structure and band gap are still under debate. As listed in Table I, a diverse range of phases, such as monoclinic, cubic, tetragonal, and hexagonal with $Cc$, $F\bar{4}3m$, $I\bar{4}2m$, and $P6_3/mmc$ symmetries, respectively, have been proposed by different groups, and so far it is not clear which structure is the ground state. For the measured band gap of CTS, different groups have also reported scattered values, from 1.35 to 0.95 eV, and to even zero (metallic) for hexagonal CTS. Once again, it is not clear what factors determine the significant differences. Without this knowledge, it is difficult to understand their influence on the properties of the synthesized CZTS and CZTSe samples or whether the ternary compounds could be considered as candidates for solar cell absorbers.

In this paper, we investigate the structural and electronic properties of CTS and CTSe using first-principles total energy and band-structure calculations, and discuss the reasons for their structural diversity observed experimentally as well as the common character in the electronic and optical properties of different phases, which we find are determined primarily by local coordination environments, while being less sensitive to long-range order.

## II. CALCULATION METHODS

The calculation is performed within the density functional formalism as implemented in the code VASP.[22] The projector augmented-wave pseudopotentials[23] are used with an energy cutoff of 400 eV for the plane-wave basis functions. The Brillouin zone integration is carried out using $8 \times 4 \times 8$ (for the monoclinic cell) or $9 \times 9 \times 3$ (for the orthorhombic cell) Monkhorst-Pack $k$-point meshes. Test calculations confirm that the total energy is converged to within 0.1 meV per atom. For the exchange-correlation functional, the generalized gradient approximation (GGA) of Perdew-Burke-Ernzerhof (PBE)[24] is used to relax the structural parameters, while the hybrid nonlocal exchange-correlation functional (HSE) is used to calculate the electronic structure and optical properties since GGA underestimates the band gap for these compounds. Previous calculations have shown that the HSE functional predicted band gaps of CZTS- and CZTSe-related compounds are in good agreement with experimental measurements.[11,25,26]

## III. CRYSTAL STRUCTURES

In Fig. 1(a), we plot the experimentally observed monoclinic structure with $Cc$ symmetry (mo-1 structure, the structural parameters are listed in Table II), which has 24 atoms in its primitive cell and is isomorphic to the structure of $Cu_2SiS_3$.[12,27] One obvious characteristic of this structure is that all S anions are tetrahedrally bonded by four cations, as in zinc-blende structure, and the structure has clear atomic layers connected by perpendicular bonds, as the (111) layers in

 

TABLE I. Structural properties (cell shape, symmetry, lattice constants $a$,$b$, and $c$ in Å) and band gaps (in eV) of CTS and CTSe reported in the literature.

| | Cell shape | Symmetry | $a$ | $b$ | $c$ | $E_g$ | Ref. |
|---|---|---|---|---|---|---|---|
| CTS | Monoclinic | $Cc$ | 6.65 | 11.54 | 6.67 | | 12 |
| CTS | Triclinic | | 6.66 | 11.48 | 20.03 | 0.95 | 13,14 |
| CTS | Cubic | | 5.43 | | | 1.15 | 15 |
| CTS | Cubic | $F\bar{4}3m$ | 5.43 | | | 0.98 | 16 |
| CTS | Tetragonal | $I\bar{4}2m$ | 5.41 | | 10.82 | | 17 |
| CTS | Tetragonal | $I\bar{4}2m$ | 5.41 | | 10.81 | 1.35 | 16 |
| CTS | Hexagonal | $P6_3/mmc$ | 3.90 | | 17.27 | 0 | 18 |
| CTSe | Monoclinic | $Cc$ | 6.95 | 12.05 | 6.97 | 0.84 | 19 and 20 |
| CTSe | Cubic | | 5.73 | | | | 21 |

the zinc-blende structure. Therefore, the monoclinic $Cu_2SnS_3$ structure with $Cc$ symmetry is in fact a superstructure of zinc blende, and its primitive cell can be described as a zinc-blende supercell with the basis vectors

$$\begin{Bmatrix} \vec{a} \\ \vec{b} \\ \vec{c} \end{Bmatrix} = \begin{Bmatrix} -0.5 & 0.5 & 1.0 \\ 1.5 & 1.5 & 0.0 \\ 0.5 & -0.5 & 1.0 \end{Bmatrix} \begin{Bmatrix} \vec{e_x} \\ \vec{e_y} \\ \vec{e_z} \end{Bmatrix}, \quad (1)$$

where $\vec{e_x}$, $\vec{e_y}$, and $\vec{e_z}$ are the basis vectors of the cubic zinc-blende conventional cell [Fig. 1(b)]. Since the kesterite structure of $Cu_2ZnSnS_4$ is also derived from a zinc-blende structure, the similarity of the complex $Cu_2SnS_3$ monoclinic structure to the simpler zinc-blende lattice is important: $Cu_2ZnSnS_4$ can be considered as a substitutional alloy of its two main secondary phases ZnS and $Cu_2SnS_3$, all having the same zinc-blende-derived lattice. Due to this similarity, the simulated x-ray diffraction (XRD) patterns for ZnS, monoclinic $Cu_2SnS_3$, and kesterite $Cu_2ZnSnS_4$ all have similar main diffractions lines,[28] which makes the distinction between the ZnS and $Cu_2SnS_3$ secondary phases in $Cu_2ZnSnS_4$ samples using diffraction techniques difficult if the crystal quality is not good enough.

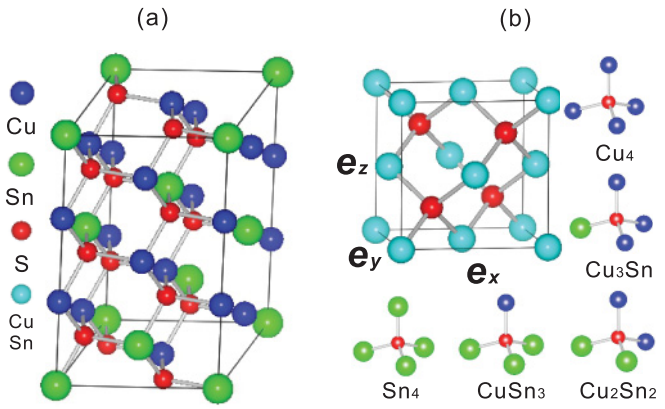


FIG. 1. (Color online) The crystal structure of $Cu_2SnS_3$: (a) monoclinic structure with $Cc$ symmetry, (b) cubic structure with $F\bar{4}3m$ symmetry (equivalent to zinc-blende structure), in which Cu and Sn are mixed on the cation sites, and there are five possible cation coordination pattern around the S anion, $Cu_4$, $Cu_3Sn$, $Cu_2Sn_2$, $CuSn_3$, and $Sn_4$, as shown by the five insets.

Besides the monoclinic structure, other structures have also been proposed by previous experiments, e.g., the cubic structure with $F\bar{4}3m$ symmetry and tetragonal structure with $I\bar{4}2m$ symmetry.[17,19,21] As we know, the *binary* zinc-blende structure has $F\bar{4}3m$ symmetry, and the *quaternary* stannite structure, which is also derived from zinc blende, has $I\bar{4}2m$ symmetry, so the ternary $Cu_2SnS_3$ can have the symmetry ($F\bar{4}3m$ or $I\bar{4}2m$) only if the cations are randomly occupied over the cation sublattice of the zinc-blende structure. In this case, the occupation of Cu or Sn cations on the atomic sites becomes fractional rather than integral. The partial occupation makes the construction of small primitive cell to model the real structure difficult. However, since all of these structures have the same underlying zinc-blende frame, and differ only in the cation arrangement, the study of their properties can be changed into the study of the influence of cation arrangement on the properties of $Cu_2SnS_3$.

To study the influence of cation arrangement, we have constructed six zinc-blende based superstructures, in which mo-1 is the monoclinic structure with $Cc$ symmetry [Fig. 1(a)] that is proposed by experiment:[12] mo-2, mo-3, and mo-4 have the same lattice vectors as mo-1 but different cation arrangements and symmetries. In fact, the mo-2 structure has an orthorhombic primitive cell with the basis vectors

$$\begin{Bmatrix} \vec{a'} \\ \vec{b'} \\ \vec{c'} \end{Bmatrix} = \begin{Bmatrix} 1.5 & 1.5 & 0.0 \\ 0.5 & -0.5 & 0.0 \\ 0.0 & 0.0 & 1.0 \end{Bmatrix} \begin{Bmatrix} \vec{e_x} \\ \vec{e_y} \\ \vec{e_z} \end{Bmatrix}, \quad (2)$$

TABLE II. The structural parameters of mo-1 and mo-2 structured $Cu_2SnS_3$: symmetry, lattice constants, angles of primitive cell, and the ideal atomic coordinates (Wyckoff positions) of the independent atoms.

| | mo-1 structure | mo-2 structure |
|---|---|---|
| Symmetry | $Cc$ | $Imm2$ |
| $a$,$b$,$c$ | 6.71, 11.62, 6.74 | 11.61, 3.92, 5.43 |
| $\alpha$,$\beta$,$\gamma$ | 90, 70.33, 90 | 90, 90, 90 |
| Cu1 | 5/12, 11/12, 1/2 (4$a$) | 5/6, 1/2, 1/2 (4$c$) |
| Cu2 | 11/12, 1/4, 0 (4$a$) | |
| Sn1 | 11/12, 11/12, 0 (4$a$) | 0, 0, 0 (2$a$) |
| S1 | 1/24, 1/12, 1/8 (4$a$) | 5/6, 0, 1/4 (4$c$) |
| S2 | 13/24, 1/12, 5/8 (4$a$) | 1/2, 0, 1/4 (2$b$) |
| S3 | 1/24, 1/4, 5/8 (4$a$) | |

TABLE III. The symmetry, amount of each cluster in the 24-atom cells, calculated lattice constants $a$, $b$, and $c$ (in Å), angle $\beta$ (in degree), and relative energy difference (meV/atom) of different $Cu_2SnS_3$ structures.

| Structure | Symmetry | $Cu_4$ | $Cu_3Sn$ | $Cu_2Sn_2$ | $CuSn_3$ | $Sn_4$ | $a$ | $b$ | $c$ | $\beta$ | $\Delta E$ |
|---|---|---|---|---|---|---|---|---|---|---|---|
| mo-1 | $Cc$ | 0 | 8 | 4 | 0 | 0 | 6.71 | 11.62 | 6.74 | 70.33 | 0.00 |
| mo-2 | $Imm2$ | 0 | 8 | 4 | 0 | 0 | 6.70 | 11.61 | 6.70 | 71.65 | −0.42 |
| mo-3 | $C2$ | 1 | 6 | 5 | 0 | 0 | 6.73 | 11.63 | 6.73 | 70.43 | 31.46 |
| mo-4 | $Pm$ | 0 | 9 | 2 | 1 | 0 | 6.71 | 11.66 | 6.75 | 71.01 | 23.66 |
| or-1 | $C222_1$ | 0 | 8 | 4 | 0 | 0 | 5.47 | 5.49 | 16.49 | 90 | 2.56 |
| or-2 | $P\bar{4}$ | 0 | 8 | 4 | 0 | 0 | 5.48 | 5.48 | 16.49 | 90 | 3.70 |

and the monoclinic cell in Eq. (1) is a supercell of mo-2 with the relationship

$$\begin{Bmatrix} \vec{a} \\ \vec{b} \\ \vec{c} \end{Bmatrix} = \begin{Bmatrix} 0 & -1 & 1 \\ 1 & 0 & 0 \\ 0 & 1 & 1 \end{Bmatrix} \begin{Bmatrix} \vec{a'} \\ \vec{b'} \\ \vec{c'} \end{Bmatrix}. \quad (3)$$

The structures or-1 and or-2 have an orthorhombic cell with $\mathbf{a} = \vec{e_x}$, $\mathbf{b} = \vec{e_y}$, $\mathbf{c} = 3\vec{e_z}$, which are constructed manually to compare with the monoclinic structures proposed by experiment. As the cation arrangement is changed, the clusters around the S anions are also changed. There are five different clusters around S, $Cu_4$, $Cu_3Sn$, $Cu_2Sn_2$, $CuSn_3$, and $Sn_4$ [shown in Fig. 1(b)]. Different structures are characterized by the symmetry and numbers of different clusters, as shown in Table III. For example, the mo-1 structure only has $Cu_3Sn$ and $Cu_2Sn_2$ clusters.

In previous studies of ternary $CuInSe_2$ and quaternary $Cu_2ZnSnS_4$ structures, the valence octet rule was found to play an important role in determining the energy stability of different structures.[7,25,29] The octet rule states that if the sum of the valence electrons of the cations surrounding the anion atom divided by the coordination number (four for tetrahedral structure) plus the number of the anion valence electrons is equal to eight, then the structure has low energy because the anion is in an eight-electron closed-shell state. For tetrahedral $Cu_2ZnSnS_4$, this requires the sum of the cation valence electrons surrounding each anion is equal to eight since S has six valence electrons. Cu, Zn, Sn, and S have one, two, four, and six valence electrons, respectively, so when S is surrounded only by two Cu, one Zn, and one Sn cations, such as those in the kesterite $Cu_2ZnSnS_4$ structure, it satisfies the octet rule, and therefore can have the lowest energy.

For $Cu_2SnS_3$, the material stoichiometry forbids ideal coordination, i.e., all tetrahedral coordination environments of S formed from Sn and Cu will deviate from the octet rule. Therefore, while none of the five clusters shown in Fig. 1(b) satisfies the octet rule completely, we can apply a generalized octet rule in which the structures with the smallest deviation from the octet rule should be favored. Furthermore, to preserve local charge neutrality, electron-rich clusters that exceed the octet rule (e.g., $Cu_2Sn_2$) should be close to electron-deficient clusters (e.g., $Cu_3Sn$). For the five clusters $Cu_4$, $Cu_3Sn$, $Cu_2Sn_2$, $CuSn_3$, and $Sn_4$, the sum of the cation valence electrons are 4, 7, 10, 13, and 16, respectively, therefore, $Cu_3Sn$ and $Cu_2Sn_2$ should be energetically favored over other clusters. In Table III, we list the abundance of these clusters for different structures. The four structures (mo-1, mo-2, or-1, and or-2) have a minimum deviation from the octet rule, i.e., they have eight $Cu_3Sn$ and four $Cu_2Sn_2$ clusters, therefore, we expect these structures have lower total energies.

The above analysis can be supported by direct first-principles total energy calculation. As shown in Table III, mo-1, mo-2, or-1, and or-2 structures have significantly lower energy than mo-3 and mo-4, indicating that in the synthesized samples only the $Cu_3Sn$ and $Cu_2Sn_2$ clusters surrounding the S anions should exist. Comparing the energy, mo-2 has slightly lower energy than mo-1 by 0.4 meV/atom. These two structures can be described by the same monoclinic cell and only have a slightly different cation occupation. The small energy difference suggests that at finite temperature the cations may be partially disordered in the cation sublattice, i.e., it has well-defined short-range order (the type of clusters around the anions) but lacking long-range order. This explains the experimentally observed structural diversity with different crystal symmetry. The situation is similar to the $CuInSe_2$-derived ordered vacancy compounds.[29] Ordered vacancy compounds are formed by creating ordered $(In_{Cu} + 2V_{Cu})$ defect pairs in $CuInSe_2$,[30] whereas $Cu_2SnS_3$ can be considered as formed by creating ordered $(Sn_{Zn} + 2Cu_{Zn})$ defect pairs in $Cu_2ZnSnS_4$.

Our analysis above indicates that the stable $Cu_2SnS_3$ structures have the following properties: (i) The basic structure is a superstructure of the zinc-blende structure, (ii) the cations occupy the fcc sublattice of the zinc-blende structure with all S anions surrounded by only $Cu_3Sn$ and $Cu_2Sn_2$ clusters, and (iii) the cation occupation may have long-range disorder at finite temperature. It should be noted that a hexagonal structure was reported previously,[18] in which the S anions are not tetrahedrally coordinated, but our total energy calculation shows that its energy is ∼500 meV/atom higher than that of the mo-1 structure, suggesting that it cannot be an energetically stable structure. Recently we have predicted wurtzite-derived (hexagonal) polytype structures (wurtzite-kesterite and wurtzite-stannite) of the quaternary CZTS, in which the S anions are tetrahedrally coordinated by two Cu, one Zn, and one Sn, and based on the similar derivation relation, we expect there may be wurtzite-derived CTS structures, but to our knowledge there have been no experimental reports about them.

Experimentally, XRD is commonly used for structural characterization, however, here we will show that it is difficult to distinguish the different cation occupations of $Cu_2SnS_3$ if the crystal quality is not good. We simulated the XRD spectrum for mo-1, mo-2, and or-1 structures (Fig. 2), in

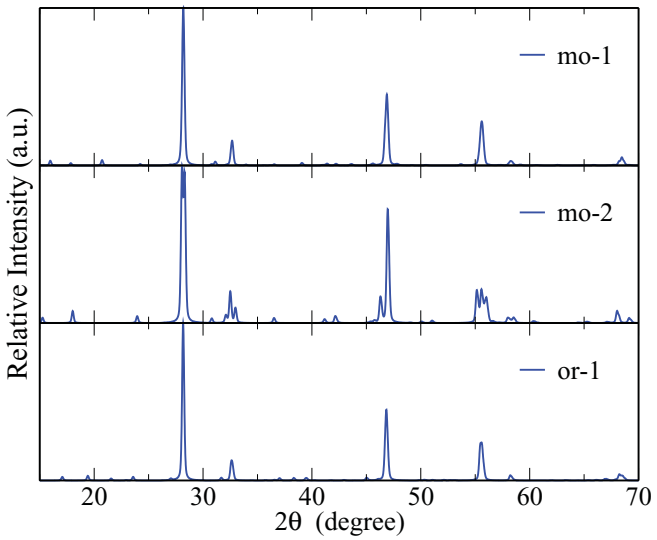


FIG. 2. (Color online) The simulated XRD spectrum of mo-1, mo-2, and or-1 structures. The nominal x-ray source is Cu $K\alpha$ ($\lambda = 0.15406$ nm).

which the positions of the main peaks all agree with the experimental measurement,[14,16] because our calculated lattice constants and bond lengths agree with experimental values. The difference in the three structures exists only in the small superstructure peaks and the splitting of main peaks, which can only be detected when the synthesized sample has high quality.

## IV. ELECTRONIC AND OPTICAL PROPERTIES

We will now study the influence of the structural diversity (cation occupations) on the electronic properties of $Cu_2SnS_3$. Because PBE exchange correlation severely underestimates the band gap, here we use the hybrid HSE functional to calculate the band structure. Figure 3 plots the calculated band structure of $Cu_2SnS_3$ and $Cu_2SnSe_3$. We can see that for this structure a direct band gap exists at the Γ point. The calculated density of states (DOS) for mo-1 and or-1 structures is plotted in Fig. 4, where the black lines show the total DOS. Comparing the DOS of mo-1 and or-1 structures, we find that they are very similar, even in the band gaps which are 0.84 eV for mo-1 and 0.88 eV for or-1 structure. This similarity is also observed for the calculated DOS of other structures with only $Cu_3Sn$ and $Cu_2Sn_2$ clusters around the S anions, indicating that the electronic structures of these compounds are insensitive to the cation distribution as long as they have the same local ordered structures.

Figure 4 also plots the partial density of states projected on Cu, Sn, and S atoms. As we can see, the valence-band maximum (VBM) is mainly the antibonding component of the hybridization between Cu *d* states and S *p* states, while the conduction-band minimum (CBM) is mainly the antibonding component of hybridization between the Sn *s* and S *s* states (this can be quantitatively seen in the component analysis of the conduction-band minimum state). This band component is similar to that of $Cu_2ZnSnS_4$, where Zn does not contribute significantly to the band edge states. Relative to $Cu_2ZnSnS_4$, which has a band gap of 1.5 eV, the creation of ordered ($Sn_{Zn}$ + $2Cu_{Zn}$) defect pairs in $Cu_2ZnSnS_4$ in forming $Cu_2SnS_3$ shifts the VBM upward because the formation of $Cu_{Zn}$ enhances the *p*-*d* repulsion, and shifts the CBM downward because the formation of $Sn_{Zn}$ makes CBM localized more on the more electronegative Sn sites,[8] therefore, decreasing the band gap of $Cu_2SnS_3$ to ∼0.8–0.9 eV. Considering different structures with the same amount of $Cu_3Sn$ and $Cu_2Sn_2$ clusters, the hybridization strength between the cation and anion states is comparable, so their band gaps differ by only a small amount, and are influenced only weakly by the long-range cation arrangement.

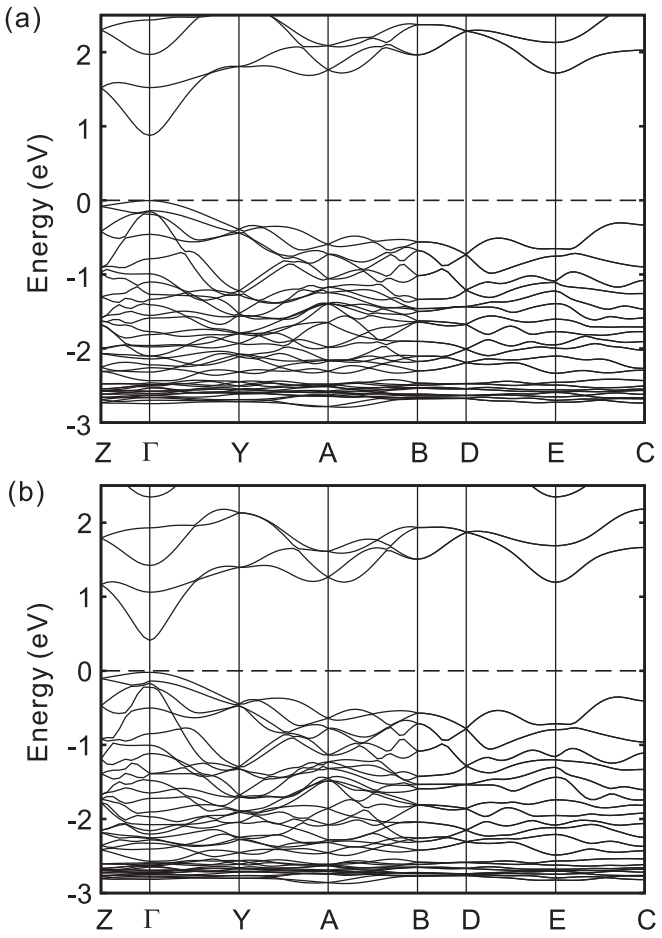


FIG. 3. The calculated band structure of mo-1 structured (a) $Cu_2SnS_3$ and (b) $Cu_2SnSe_3$. The energy zero is set to the top of the valence band.

Comparing the calculated band gaps of CTS with the measured values listed in Table I, we find that the calculated values 0.8–0.9 eV agrees reasonably well with experiment (0.95–1.35 eV), considering the calculation uncertainty and the fact that the absorption measurement often overestimates the band gap, especially for samples with poor quality.[15,16] The zero band gap (metallic) observed in Ref. 18 may result from the nontetrahedral structure of the synthesized CTS sample, but as aforementioned, this structure is highly unstable; otherwise, a highly nonstoichiometric material may have been formed. Considering the scattered band gap values in previous experimental literature, further accurate experimental measurement is called for.

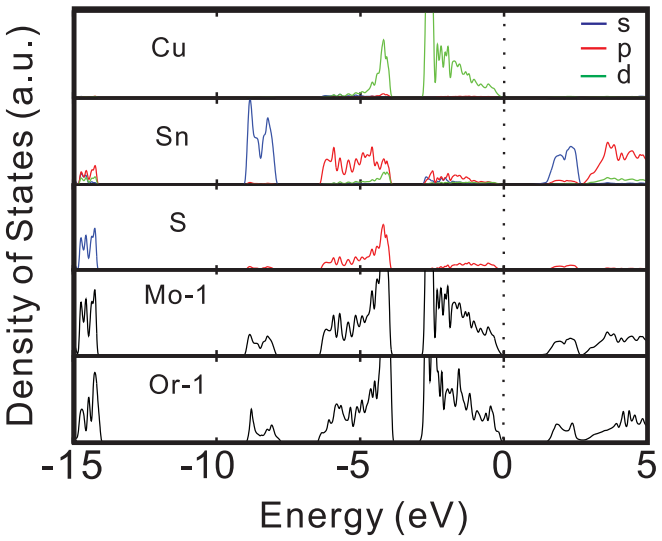


FIG. 4. (Color online) The partial and total electronic density of states for $Cu_2SnS_3$ in mo-1 and or-1 structures.

As CTS has a substantially smaller band gap than CZTS, and their structures and lattice constants are highly compatible, we expect that CTS may be used as a cheap bottom layer and CZTS as middle layer materials in low-cost multijunction solar cells.

Turning to the selenide material, $Cu_2SnSe_3$ can be a secondary phase in synthesized CZTSe samples. Our calculations have shown that it has a similar crystal structure and density of states as CTS, but its band gap is relatively smaller, with values of only 0.39 eV for the mo-1 structure and 0.40 eV for the or-1 structure. The smaller gap of CTSe than CTS is similar to the situation between CZTSe (band gap 1.0 eV) and CZTS (band gap 1.5 eV), which can be understood considering two factors: (i) Se has a higher 4*p* level than the S 3*p* level, so the valence band of CTSe is higher than CTS, and (ii) Sn-Se bond length is larger than the Sn-S bond, thus the *s*-*s* hybridization is weaker, shifting down the conduction band of CTSe. Comparing with the experimental value 0.84 eV in Refs. 19 and 20, the calculated band gap is much smaller. This disagreement between calculations and experiments has also existed in CZTSe systems before, where earlier absorption spectrum measurements reported band gap sizes ∼1.5 eV, much larger than our calculated value of 1.0 eV.[25] However, our calculated value was confirmed by recent experimental measurements.[11] The large uncertainty in the band-gap measurement for these compounds comes partially from the high defect density and poor crystal quality.

In Fig. 5, we plot the imaginary part of the calculated dielectric functions for CTS and CZTS, as well as for CTSe and CZTSe, where all the diagonal elements are averaged. The calculated result for CZTS is in good agreement with that obtained in Ref. 26. The overall shape is similar for CTS (CTSe) and CZTS (CZTSe), due to their similar band component near the gap, but the energy threshold from zero to nonzero dielectric function is redshifted for CTS than CZTS, which represents the band-gap sizes. As the imaginary part of the dielectric function is closely related to the absorption coefficient, the similar dielectric function of CTS and CZTS

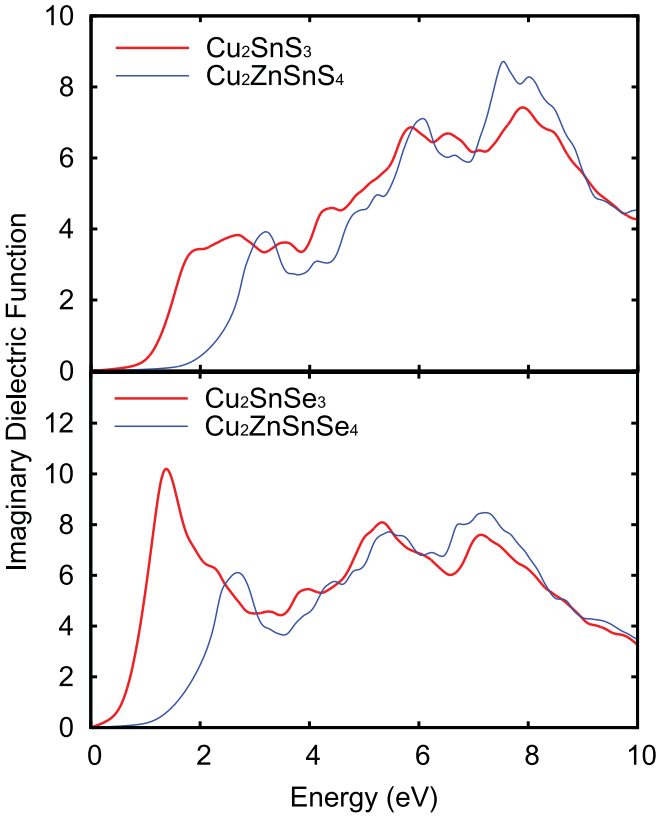


FIG. 5. (Color online) The calculated imaginary dielectric function of $Cu_2SnS_3$ and $Cu_2ZnSnS_4$ (top panel), and $Cu_2SnSe_3$ and $Cu_2ZnSnSe_4$ (bottom panel) using the HSE functional.

indicates their absorption of light is also comparable, differing only in the onset-to-absorption frequency. According to the calculated results, the alloying of CTS with CZTS should cause the change in the absorption spectrum with a redshift of the absorption curve, and this feature could be used for band-structure engineering for solar-cell designs if the synthesis can be controlled.

## V. CONCLUSIONS

In conclusion, we have studied the structural and electronic properties of CTS and CTSe using a first-principles electronic structure approach. We have found that their stable structures are all derived from the zinc-blende structure with all anions tetrahedrally coordinated by $Cu_3Sn$ and $Cu_2Sn_2$, but may contain long-range cation disorder at finite temperature. The structural preferences can be rationalized in terms of a generalized valence octet rule. Our calculations predict that CTS and CTSe have similar optical properties to those of CZTS and CZTSe, but their direct band gaps are smaller (0.9 and 0.4 eV, respectively), and are weakly influenced by the long-range cation ordering. These low band-gap materials maybe be suitable for extending the visible light absorption of low-cost thin-film solar cells based on CZTS.

## ACKNOWLEDGMENTS

This work is supported by NSF of China (No. 10934002 and No. 10950110324) and Shanghai (No. 10ZR1408800),

the Research Program of Shanghai municipality and MOE, the Special Funds for Major State Basic Research, CC of ECNU and the Fundamental Research Funds for the Central Universities. A.W. acknowledges membership in the UK HPC Materials Chemistry Consortium, which is funded by EPSRC (Grant No. EP/F067496). The work at NREL is funded by the US Department of Energy, EERE, under Contract No. DE-AC36-08GO28308.

[1]Q. Guo, G. M. Ford, W. C. Yang, B. C. Walker, E. A. Stach, H. W. Hillhouse, and R. Agrawal, J. Am. Chem. Soc. **132**, 17384 (2010).
[2]K. Wang, O. Gunawan, T. Todorov, B. Shin, S. J. Chey, N. A. Bojarczuk, D. Mitzi, and S. Guha, Appl. Phys. Lett. **97**, 143508 (2010).
[3]Q. Guo, H. W. Hillhouse, and R. Agrawal, J. Am. Chem. Soc. **131**, 11672 (2009).
[4]A. Shavel, J. Arbiol, and A. Cabot, J. Am. Chem. Soc. **132**, 4514 (2010).
[5]A. Weber, S. Schmidt, D. Abou-Ras, P. Schubert-Bischoff, I. Denks, R. Mainz, and H. W. Schock, Appl. Phys. Lett. **95**, 041904 (2009).
[6]J. J. Scragg, P. J. Dale, L. M. Peter, G. Zoppi, and I. Forbes, Phys. Status Solidi B **245**, 1772 (2008).
[7]S. Chen, X. G. Gong, A. Walsh, and S.-H. Wei, Appl. Phys. Lett. **96**, 021902 (2010).
[8]S. Chen, J. H. Yang, X. G. Gong, A. Walsh, and S.-H. Wei, Phys. Rev. B **81**, 245204 (2010).
[9]K. Wang, B. Shin, K. B. Reuter, T. Todorov, D. B. Mitzi, and S. Guha, Appl. Phys. Lett. **98**, 051912 (2011).
[10]A. Redinger, K. Hoenes, X. Fontane, V. Izquierdo Roca, E. Saucedo, N. Valle, A. Perez-Rodriguez, and S. Siebentritt, Appl. Phys. Lett. **98**, 101907 (2011).
[11]S. Ahn, S. Jung, J. Gwak, A. Cho, K. Shin, K. Yoon, D. Park, H. Cheong, and J. H. Yun, Appl. Phys. Lett. **97**, 021905 (2010).
[12]M. Onoda, X. A. Chen, A. Sato, and H. Wada, Mater. Res. Bull. **35**, 1563 (2000).
[13]X. Chen, X. Wang, C. An, J. Liu, and Y. Qian, J. Cryst. Growth **256**, 368 (2003).
[14]D. Avellaneda, M. T. S. Nair, and P. K. Nair, J. Electrochem. Soc. **157**, D346 (2010).
[15]M. Bouaziz, M. Amlouk, and S. Belgacem, Thin Solid Films **517**, 2527 (2009).
[16]P. A. Fernandes, P. M. P. Salomé, and A. F. da Cunha, Physica Status Solidi C **7**, 901 (2010).
[17]X. A. Chen, H. Wada, A. Sato, and M. Mieno, J. Solid State Chem. **139**, 144 (1998).
[18]C. Wu, Z. Hu, C. Wang, H. Sheng, J. Yang, and Y. Xie, Appl. Phys. Lett. **91**, 143104 (2007).
[19]G. E. Delgado, A. J. Mora, G. Marcano, and C. Rincón, Mater. Res. Bull. **38**, 1949 (2003).
[20]G. Marcano, C. Rincón, L. M. de Chalbaud, D. B. Bracho, and G. S. Pérez, J. Appl. Phys. **90**, 1847 (2001).
[21]G. S. Babu, Y. K. Kumar, Y. B. K. Reddy, and V. S. Raja, Mater. Chem. Phys. **96**, 442 (2006).
[22]G. Kresse and J. Furthmüller, Comput. Mater. Sci. **6**, 15 (1996).
[23]G. Kresse and D. Joubert, Phys. Rev. B **59**, 1758 (1999).
[24]J. P. Perdew, K. Burke, and M. Ernzerhof, Phys. Rev. Lett. **77**, 3865 (1996).
[25]S. Chen, X. G. Gong, A. Walsh, and S.-H. Wei, Appl. Phys. Lett. **94**, 041903 (2009).
[26]J. Paier, R. Asahi, A. Nagoya, and G. Kresse, Phys. Rev. B **79**, 115126 (2009).
[27]I. D. Olekseyuk, L. V. Piskach, O. Y. Zhbankov, O. V. Parasyuk, and Y. M. Kogut, J. Alloys Compd. **399**, 149 (2005).
[28]S. Chen, X. G. Gong, A. Walsh, and S. H. Wei (unpublished).
[29]C. H. Chang, S.-H. Wei, J. W. Johnson, S. B. Zhang, N. Leyarovska, G. Bunker, and T. J. Anderson, Phys. Rev. B **68**, 054108 (2003).
[30]S. B. Zhang, S.-H. Wei, and A. Zunger, Phys. Rev. Lett. **78**, 4059 (1997).